Femtosecond-laser micromachined optical waveguides in $Bi_4Ge_3O_{12}$ crystals

Ruiyun He,[1] Qiang An,[1] Javier R. Vázquez de Aldana,[2] Qingming Lu,[3] and Feng Chen[1],*

[1]School of Physics, State Key Laboratory of Crystal Materials and Key Laboratory of Particle Physics and Particle Irradiation (Ministry of Education), Shandong University, Jinan 250100, China

[2]Laser Microprocessing Group, Departamento de Física Aplicada, Universidad de Salamanca, Salamanca 37008, Spain

[3]School of Chemistry and Chemical Engineering, Shandong University, Jinan 250100, China

*Corresponding author: drfchen@sdu.edu.cn

The optical waveguides in $Bi_4Ge_3O_{12}$ (BGO) crystals in both depressed-cladding and dual-line configurations have been produced using femtosecond-laser micromachining. The guiding properties and thermal stabilities of the BGO waveguides have been investigated for both geometries, showing different performance of the fabricated structures. Both depressed-cladding and dual-line waveguides support guidance along both TE and TM polarizations. Thermal annealing treatments up to 600°C reduce the propagation loss of dual-line waveguides to as low as 0.5 dB/cm, while the cladding waveguide is only stable under thermal treatment not higher than 260°C, reaching a propagation loss of 2.1 dB/cm. © 2013 Optical Society of America

OCIS codes: (230.7370) Waveguides; (320.7130) Ultrafast processes in condensed matter, including semiconductors; (130.0130) Integrated optics.

http://dx.doi.org/10.1364/AO.52.003713

1. Introduction

In integrated photonics, optical waveguides, as basic components, can confine the light propagation in small volumes, in which relatively high optical intensities could be achieved. Such structures offer the feasibility to construct compact platforms in single circuits, which can be applied to realize a few photonic applications [1]. Several techniques have been developed to produce optical waveguides in materials, such as thermal ion indiffusion [2], ion implantation/irradiation [3], ion exchange [4], and femtosecond (fs) laser micromachining [5]. Fs-laser micromachining has been applied to fabricate waveguides with diverse geometries in various transparent materials, such as glasses, single crystals, ceramics, and polymers [6–11]. This technique has some unique features in three-dimensional (3D) microstructuring of materials with high spatial resolution. By tightly focusing the fs-laser beams into the bulk of the transparent material, the refractive index modification of a small volume could be induced. The performance of the waveguides fabricated by fs-laser inscription depends on not only the material properties but also the parameters of micromachining, such as pulse duration and energy, scan speed, repetition rate, focal depth, and polarization [12–15]. By using fs-laser micromachining, waveguides with diverse configurations may be constructed. In the so-called type I waveguides, the fs-laser irradiated tracks have positive refractive index changes, resulting in waveguides located inside the filaments. Such geometry is common in fs-laser-inscribed waveguides in glasses [16–19]. Type II waveguides, namely stress-induced structures, are usually fabricated by the dual-line

technique [20,21], which creates negative index changes in the parallel tracks; as a result of strain field modifications, the waveguide will be constructed in the region between two tracks. This technique has been utilized to fabricate waveguides in a number of crystals. In addition, depressed-cladding waveguides could be fabricated by the fs-laser inscription as well, whose guiding core is normally surrounded by a number of low-index tracks [22–26]. In a 3D view, the cladding waveguides look like photonic tubes typically with circular cross-sectional shapes, and the diameters of the structures could be designed from 30 to 200 μm. This offers the tubular structures the guidance of light at wavelength regimes from visible to mid-infrared. Nevertheless, boundaries with any shapes can theoretically be constructed to form cladding waveguides. For instance, hexagonal, circular, and trapezoidal waveguides have been successfully fabricated in Nd:YAG ceramics by Liu *et al.* [26]. Particularly, since circular-shaped cross sections with desired diameters could be designed to fit well the optical fibers, it is also promising to realize the integration of the fiber-waveguide photonic system by using the cladding structures.

Bismuth germanate ($Bi_4Ge_3O_{12}$ or BGO) is a well-known scintillating crystal with cubic structure [27]. The features of BGO crystal, such as its nonhygroscopic nature, its high electro-optic coefficient, and its easy preparation, make it an ideal crystal for nuclear physics, space physics, nuclear medicine, high-energy physics, and other fields. In early works, BGO waveguides were fabricated by ion implantation and swift ion irradiation [28–31], and the guiding characteristic and the effect of the annealing treatment were investigated. Fs-laser micromachining was utilized to fabricate waveguides in BGO crystal with a dual-line approach [32]. The work showed the possibility and advantages of using BGO waveguide arrays to replace the BGO segments in positron emission tomography systems. However, the propagation loss of the dual-line type II waveguides in BGO was as high as 4.2 dB/cm.

In this work, we report, to our best knowledge for the first time, on the fabrication of depressed-cladding waveguides in BGO crystal. The dual-line waveguides in BGO crystal were produced using fs-laser micromachining as well. The optical guiding properties in different polarizations and thermal stabilities of the fabricated BGO waveguides are investigated. Particularly, it will be proved that the propagation loss of the dual-line waveguide could be reduced to as low as ~0.5 dB/cm after relatively high temperature annealing.

2. Experimental Details

The BGO crystal used in this work was cut with a size of 10 mm × 9.5 mm × 2 mm and optically polished. One cladding waveguide with a circular boundary and four type II waveguides with dual-line structures were produced using the laser facility of

Table 1. Fabrication Parameters of BGO Waveguides by Fs-Laser Micromachining

Waveguides	Pulse Energy (μJ)	Scan Velocity (μm/s)	Separation (μm)
Depressed cladding	1.68	500	3
Dual-line No. 1	1.68	50	15
Dual-line No. 2	1.68	50	20
Dual-line No. 3	2.52	50	15
Dual-line No. 4	2.52	50	20

the Universidad de Salamanca, Spain. We used a Ti:sapphire laser system generating 120 fs pulses, linearly polarized at 800 nm and with a low repetition rate of 1 kHz. The precise value of pulse energy used to irradiate the sample was set with a calibrated neutral density filter, a half-wave plate, and a linear polarizer. The sample was located at a three-axes motorized stage, and the beam was focused through the largest sample surface (dimensions 9.5 mm × 10 mm) at a depth of ~125 μm by a 40 × microscope objective (N.A. = 0.65) to produce damage filaments. Table 1 shows the fabrication parameters of the circular cladding and four dual-line waveguides, including their pulse energy and scan velocity, and the separation between two neighboring tracks.

The microscope images of the waveguide cross sections were taken using a polarized microscope (Axio Imager, Carl Zeiss). The near-field modal investigation was performed using a typical end-face arrangement with a linearly polarized He–Ne laser at a wavelength of 632.8 nm, as shown in Fig. 1. A pair of microscope objective lenses (25×) was used to couple the laser into and out of the waveguides. Afterward, we used a CCD camera, which was connected to a computer, to record the data. Based on the above arrangement, the waveguide propagation losses were estimated by directly measuring the incident and output light powers of the waveguides. Furthermore, the sample was annealed in an open oven to improve the waveguide qualities and investigate the thermal stabilities. We processed a series of thermal annealing treatments, at 260°C, 260°C, 360°C, 500°C, and 600°C in sequence, for 1 h each step. In this work, they were labeled steps 1–5, respectively. The guiding properties and propagation losses were measured after each step.

3. Results and Discussion

A. Microscope Images

Figures 2(a) and 2(b) show the optical microscope images of the cross sections of the BGO cladding and
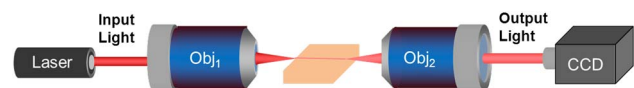

Fig. 1. Schematic of the end-face coupling arrangement applied to investigate the near-field intensity distributions of the BGO waveguides.
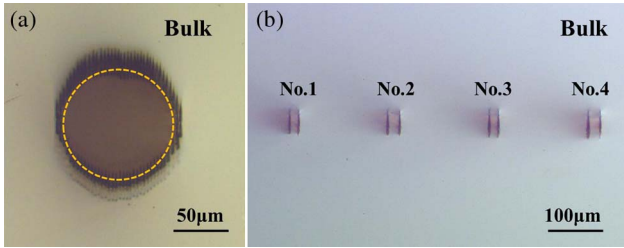
Fig. 2. Optical microscope images of the cross sections of (a) cladding and (b) dual-line BGO waveguides Nos. 1–4. The dashed line indicates the location of the cladding waveguide.

Fig. 4. Measured near-field intensity distributions of dual-line waveguides Nos. 1–4 for both TE (top) and TM (bottom) polarizations at 632.8 nm.

dual-line waveguides, respectively. The diameter of the cross-sectional circle of the cladding waveguide is ~100 μm. The waveguide core is located in the region that is surrounded by a number of fs-laser-inscribed tracks. As depicted in Fig. 2(b), the dual-line structures contain two filaments with separations of 15, 20, 15, and 20 μm for waveguides Nos. 1, 2, 3, and 4, respectively. The type II stress-induced BGO waveguides are located between these two filaments.

B. Modal Profiles

Figures 3(a) and 3(b) show the measured near-field mode distributions along TE and TM polarizations of the circular cladding waveguide, respectively, at the wavelength of 632.8 nm. As one can see, the cladding waveguide has similar modal profiles for TE and TM modes. And both TE and TM modes are highly multimode, which is in agreement with the theoretical estimation from the guided-wave optics. Figures 4(a)–4(h) depict the measured near-field modal profiles of the TE and TM modes of dual-line BGO waveguides Nos. 1–4, respectively, at the wavelength of 632.8 nm. As one can see, the mode distributions of the dual-line waveguides are nearly single mode. However, as mentioned in the previous work [12,33], the guiding of dual-line waveguides fabricated by fs-laser micromachining in other cubic crystals, such as Nd:YAG and Nd:GGG, was only possible when the polarization of the incident light was parallel to the long axis of the cross section of the written tracks, i.e., the TM polarization in our work. The refractive index alternations inside the sample, as is discussed in Section 3.C, make it possible to guide light along both TE and TM polarizations in the
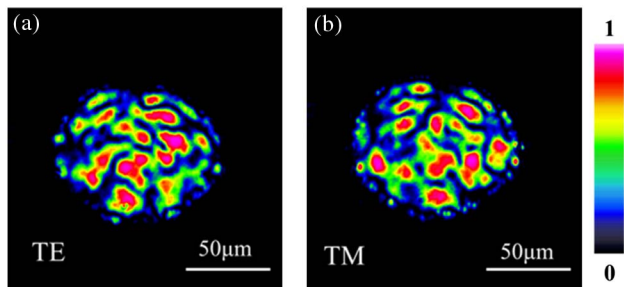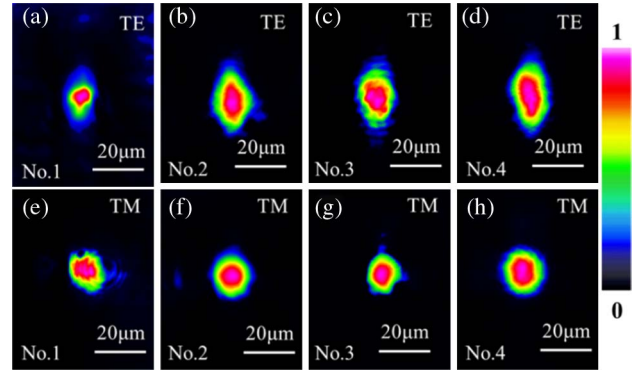
BGO dual-line waveguides. This difference of guidance in BGO waveguides with other cubic crystals such as Nd:YAG may be due to the discrepancy of detailed atomic coordination in lattices of different materials. Nevertheless, it still needs more detailed investigation on the specific mechanism and influencing factors for deeper understanding.

C. Refractive Index Profiles

We used the numerical aperture method [13] to estimate the refractive index contrasts between the damage lines and the waveguide region of type II BGO waveguides. In this work, a step-like profile was assumed to demonstrate the refractive index distribution of the type II waveguide. We measured the maximum incident angle Θ_m at which no change of the transmitted power was occurring. With this value, the maximum index change in the waveguide could be obtained using the formula

$$\Delta n \approx \frac{\sin^2 \Theta_m}{2n}, \qquad (1)$$

where n is the refractive index of the bulk. In this work, the calculated maximum refractive index alternations were ~9.4×10^{-4}, ~9.8×10^{-4}, ~9.7×10^{-4}, and ~1.86×10^{-3} for the TM modes of BGO dual-line waveguides Nos. 1–4, respectively.

With the obtained Δn, one can reconstruct the two-dimensional (2D) refractive index profiles of the dual-line BGO waveguides using the technique introduced in previous works [33]. Since the four profiles are similar, we simply exhibit one for brevity. Figure 5(a) shows the reconstructed 2D refractive index profile at the cross section of dual-line BGO waveguide No. 4 of the TM polarization. As one can see, a positive index change $\Delta n_{core} = +4.6 \times 10^{-4}$ appeared in the waveguide core, which may due to the fs-laser-induced stress effect [34], while inside the two filaments, there was a refractive index decrease of $\Delta n_{track} = -1.4 \times 10^{-3}$. According to the reconstructed 2D refractive index profile, we simulated the light propagation in the waveguide

Fig. 3. Measured near-field intensity distributions of (a) TE and (b) TM modes of the circular cladding waveguide at 632.8 nm.
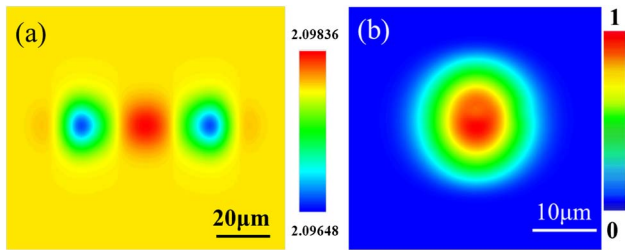
Fig. 5. (a) Reconstructed 2D refractive index profile at the cross section and (b) calculated modal profile of dual-line BGO waveguide No. 4 of TM polarization at 632.8 nm.

using the computer software Rsoft, based on the finite-difference beam-propagation method [35,36]. Figure 5(b) shows the calculated modal profile of dual-line waveguide No. 4 along the TM polarization in BGO crystal. By comparing Fig. 4(h) with Fig. 5(b), one can see that the calculated profile is in good agreement with the experimental result, which proves that the reconstructed refractive index profile of the dual-line waveguide is reasonable. In addition, for the depressed-cladding waveguide, the expected refractive index distribution may be similar to that of fs-laser-inscribed ZnS cladding waveguides [37].

D. Propagation Losses and Thermal Stabilities

For the circular cladding waveguide, the coupling and propagation losses were estimated to be ~1.2 dB and ~3.7 dB/cm, and no obvious difference was found between TE and TM modes. The propagation loss decreased to ~3.1 and ~2.1 dB/cm after annealing treatment steps 1 and 2. In step 3, the guiding performance became poor, which showed up as an increase in the propagation loss. In addition, after steps 4 and 5, the waveguide structure was difficult to maintain. As one can see, the first two steps of annealing at 260°C were effective for enhancing the guiding quality of the circular cladding waveguide. We suggested that the first two steps lessen the lattice defects and disorder induced during the inscription process. However, it seems that after annealing at higher temperatures, i.e., at 360°C, 500°C, and 600°C, used in this work, the damage-induced stress fields were changed significantly, resulting in the lattice recovering to a certain extent; consequently, the refractive index of the damaged tracks was close to its bulk value, which led to removal of the waveguide.

The coupling losses of the dual-line BGO waveguides, by calculating the overlap of the incident beam and the waveguide modal fields, were estimated to be ~1.7 and ~2.7 dB for those with separation of 15 and 20 μm, respectively. For the dual-line BGO waveguides (as irradiated by the fs lasers) along TE polarization, the propagation losses were measured to be as high as ~26.1, ~12.7, ~20.5, and ~11.1 dB/cm for Nos. 1–4, respectively. The annealing treatment step 1 was effective to reduce the propagation losses to ~17.0, ~10.9, ~16.4, and

~8.8 dB/cm, respectively. After step 2, with the same annealing temperature 260°C of step 1, the propagation losses had no obvious changes, showing thermal stability. Nevertheless, after the following annealing steps, the confinement in TE polarization became too poor to maintain the guiding of light, which was in accordance with the estimation from guided-wave optics and the results of other cubic crystals.

By comparison, the qualities of the TM modes of four dual-line BGO waveguides were superior to those of the TE modes, which could be deduced from Fig. 6. As irradiated by the fs lasers, the propagation losses were ~22.2, ~11.5, ~17.6, and ~6.9 dB/cm for dual-line waveguides Nos. 1–4, respectively. After annealing step 1, the values were reduced significantly to ~16.9, ~9.2, ~15.5, and ~5.0 dB/cm, while in the further annealing treatment steps 2 and 3, the changes were very slight, exhibiting good stability. Moreover, as one can see, the values were a little smaller than the corresponding values of TE modes, except waveguide No. 4, for which the TM mode was much better than the TE mode. Nevertheless, the results, shown in the following annealing treatments of the TM modes, are meaningful and useful. The propagation losses declined obviously at the higher temperatures 500°C and 600°C and reached ~6.0, ~1.0, ~3.8, and ~0.5 dB/cm for dual-line waveguides Nos. 1–4, respectively. The propagation loss of the type II BGO waveguide fabricated by Qian *et al.* [32] was estimated to be 4.2 dB/cm, which was much smaller than the values of the dual-line waveguides in this work obtained as fs-laser inscribed. However, we want to point out that the propagation losses were reduced by as high as 70% and 90% for the type II BGO waveguide with separations of 15 and 20 μm, respectively, by processing a series of annealing treatments. Particularly, the propagation loss of type II BGO waveguide No. 4 was reduced as low as ~0.5 dB/cm.
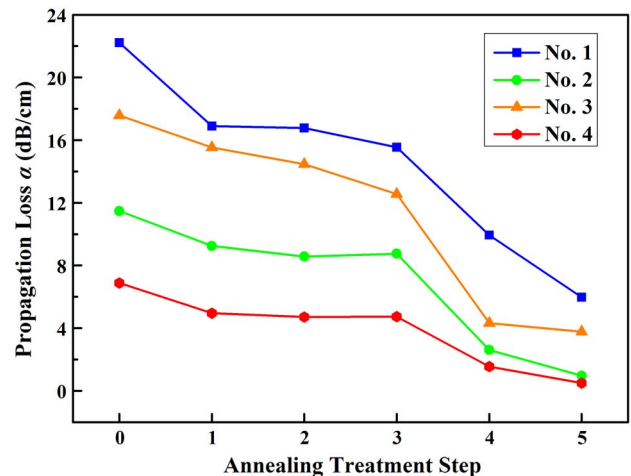

Fig. 6. Propagation losses α of the TM modes of dual-line BGO waveguides Nos. 1–4 before and after thermal annealing treatments.

We analyzed the effect of the different preparation parameters on the waveguide propagation qualities. According to the value of the propagation losses α increasing, we can make a conclusion that $\alpha_4 < \alpha_2 < \alpha_3 < \alpha_1$. Waveguides No. 2 and No. 4 with separation of 20 μm were superior to No. 1 and No. 3 of 15 μm. Furthermore, as for the two with the same separation, the one with a higher pulse energy had a lower loss, i.e., $\alpha_4 < \alpha_2$ and $\alpha_3 < \alpha_1$, which might because the stress and damage of the laser-modified filaments were larger in the higher pulse energy, 2.52 μJ.

The repetition rate of the laser used in this work was 1 kHz, which means that the time between pulses is long enough so that the thermal diffusion has carried the heat away from the focus before the next pulse arrives and the ensuing pulses act independently of one another [38]. In this situation, we suggest that the different scan velocities signify different densities of pulses. Because the scan velocity of the filaments surrounding the circular cladding waveguide was 500 μm/s, the stress and damage induced by fs-laser inscription were smaller for those dual-line filaments with a scan velocity of 50 μm/s. This might be the reason that the guiding properties of the type II BGO waveguides preserved better than the circular cladding BGO waveguide after a series of thermal annealing treatments.

As discussed above, the fabrication parameters during the fs-laser micromachining process have various influences on waveguide performance, which means we can improve the guide qualities by optimizing the preparation parameters. Pulse energy is a key factor to consider. It is also useful to find proper separations between neighboring tracks for not only dual-line but also cladding waveguides. We suggest that a reasonably lower scan velocity could create more damage that contributes to refractive index changes. Thus one can choose the appropriate scan velocity, taking both the guiding properties and the practical requirement into account.

4. Conclusions

We report on the fabrication of depressed-cladding waveguides and dual-line waveguides in BGO crystal using fs-laser micromachining. The circular cladding waveguide with a diameter of ~100 μm supports good guidance in both TE and TM polarizations. For the dual-line waveguides, single modes are achieved for both TE and TM modes, though the TM modes are far superior to the TE modes. The thermal annealing treatment we performed to improve the guiding qualities is effective to reduce the propagation loss of dual-line waveguides to 0.5 dB/cm. The high-quality guiding properties we found suggest promising applications to BGO guiding devices in integrated optics.

References

1. F. Chen, "Micro- and submicrometric waveguiding structures in optical crystals produced by ion beams for photonic applications," Laser Photon. Rev. **6**, 622–640 (2012).
2. D. Jaque, E. Cantelar, and G. Lifante, "Lattice micro-modifications induced by Zn diffusion in Nd:LiNbO$_3$ channel waveguides probed by Nd^{3+} confocal micro-luminescence," Appl. Phys. B **88**, 201–204 (2007).
3. G. B. Montanari, P. De Nicola, S. Sugliani, A. Menin, A. Parini, A. Nubile, G. Bellanca, M. Chiarini, M. Bianconi, and G. G. Bentini, "Step-index optical waveguide produced by multistep ion implantation in LiNbO$_3$," Opt. Express **20**, 4444–4453 (2012).
4. A. Tervonen, B. R. West, and S. Honkanen, "Ion-exchanged glass waveguide technology: a review," Opt. Eng. **50**, 071107 (2011).
5. R. R. Gattass and E. Mazur, "Femtosecond laser micromachining in transparent materials," Nat. Photonics **2**, 219–225 (2008).
6. L. B. Fletcher, J. J. Witcher, N. Troy, S. T. Reis, R. K. Brow, and D. M. Krol, "Direct femtosecond laser waveguide writing inside zinc phosphate glass," Opt. Express **19**, 7929–7936 (2011).
7. Y. Tan, Y. C. Jia, F. Chen, J. R. Vázquez de Aldana, and D. Jaque, "Simultaneous dual-wavelength lasers at 1064 and 1342 nm in femtosecond-laser-written Nd:YVO$_4$ channel waveguides," J. Opt. Soc. Am. B **28**, 1607–1610 (2011).
8. A. Rodenas and A. K. Kar, "High-contrast step-index waveguides in borate nonlinear laser crystals by 3D laser writing," Opt. Express **19**, 17820–17833 (2011).
9. T. Calmano, J. Siebenmorgen, O. Hellmig, K. Petermann, and G. Huber, "Nd:YAG waveguide laser with 1.3 W output power, fabricated by direct femtosecond laser writing," Appl. Phys. B **100**, 131–135 (2010).
10. T. Calmano, A. G. Paschke, J. Siebenmorgen, S. T. Fredrich-Thornton, H. Yagi, K. Petermann, and G. Huber, "Characterization of an Yb:YAG ceramic waveguide laser, fabricated by the direct femtosecond-laser writing technique," Appl. Phys. B **103**, 1–4 (2011).
11. L. Kallepalli, V. Soma, and N. Desai, "Femtosecond-laser direct writing in polymers and potential applications in microfluidics and memory devices," Opt. Eng. **51**, 073402 (2012).
12. J. Siebenmorgen, K. Petermann, G. Huber, K. Rademaker, S. Nolte, and A. Tünnermann, "Femtosecond laser written stress-induced Nd:Y$_3$Al$_5$O$_{12}$ (Nd:YAG) channel waveguide laser," Appl. Phys. B **97**, 251–255 (2009).
13. S. M. Eaton, H. Zhang, M. L. Ng, J. Li, W. J. Chen, S. Ho, and P. R. Herman, "Transition from thermal diffusion to heat accumulation in high repetition rate femtosecond laser writing of buried optical waveguides," Opt. Express **16**, 9443–9458 (2008).
14. M. Will, S. Nolte, B. N. Chichkov, and A. Tünnermann, "Optical properties of waveguides fabricated in fused silica by femtosecond laser pulses," Appl. Opt. **41**, 4360–4364 (2002).
15. M. Ams, G. D. Marshall, and M. J. Withford, "Study of the influence of femtosecond laser polarisation on direct writing of waveguides," Opt. Express **14**, 13158–13163 (2006).
16. K. M. Davis, K. Miura, N. Sugimoto, and K. Hirao, "Writing waveguides in glass with a femtosecond laser," Opt. Lett. **21**, 1729–1731 (1996).
17. N. D. Psaila, R. R. Thomson, H. T. Bookey, S. Shen, N. Chiodo, R. Osellame, G. Cerullo, A. Jha, and A. K. Kar, "Supercontinuum generation in an ultrafast laser inscribed chalcogenide glass waveguide," Opt. Express **15**, 15776–15781 (2007).
18. C. Mauclair, A. Mermillod-Blondin, N. Huot, E. Audouard, and R. Stoian, "Ultrafast laser writing of homogeneous longitudinal waveguides in glasses using dynamic wavefront correction," Opt. Express **16**, 5481–5492 (2008).

19. T. T. Fernandez, G. D. Valle, R. Osellame, G. Jose, N. Chiodo, A. Jha, and P. Laporta, "Active waveguides written by femtosecond laser irradiation in an erbium-doped phospho-tellurite glass," Opt. Express **16**, 15198–15205 (2008).

20. N. N. Dong, Y. Tan, A. Benayas, J. Vázquez de Aldana, D. Jaque, C. Romero, F. Chen, and Q. M. Lu, "Femtosecond laser writing of multifunctional optical waveguides in a Nd:YVO$_4$ + KTP hybrid system," Opt. Lett. **36**, 975–977 (2011).

21. G. A. Torchia, A. Rodenas, A. Benayas, E. Cantelar, L. Roso, and D. Jaque, "Highly efficient laser action in femtosecond-written Nd:yttrium aluminum garnet ceramic waveguides," Appl. Phys. Lett. **92**, 111103 (2008).

22. D. G. Lancaster, S. Gross, H. Ebendorff-Heidepriem, K. Kuan, T. M. Monro, M. Ams, A. Fuerbach, and M. J. Withford, "Fifty percent internal slope efficiency femtosecond direct-written Tm^{3+}:ZBLAN waveguide laser," Opt. Lett. **36**, 1587–1589 (2011).

23. Y. C. Jia, J. R. Vázquez de Aldana, C. Romero, Y. Y. Ren, Q. M. Lu, and F. Chen, "Femtosecond-laser-inscribed BiB$_3$O$_6$ nonlinear cladding waveguide for second-harmonic generation," Appl. Phys. Express **5**, 072701 (2012).

24. A. G. Okhrimchuk, A. V. Shestakov, I. Khrushchev, and J. Mitchell, "Depressed cladding, buried waveguide laser formed in a YAG:Nd^{3+} crystal by femtosecond laser writing," Opt. Lett. **30**, 2248–2250 (2005).

25. A. Okhrimchuk, V. Mezentsev, A. Shestakov, and I. Bennion, "Low loss depressed cladding waveguide inscribed in YAG:Nd single crystal by femtosecond laser pulses," Opt. Express **20**, 3832–3843 (2012).

26. H. L. Liu, Y. C. Jia, J. R. Vázquez de Aldana, D. Jaque, and F. Chen, "Femtosecond laser inscribed cladding waveguides in Nd:YAG ceramics: fabrication, fluorescence imaging and laser performance," Opt. Express **20**, 18620–18629 (2012).

27. W. Drozdowski, A. J. Wojtowicz, S. M. Kaczmarek, and M. Berkowski, "Scintillation yield of Bi$_4$Ge$_3$O$_{12}$ (BGO) pixel crystals," Physica B **405**, 1647–1651 (2010).

28. S. M. Mahdavi, P. J. Chandler, and P. D. Townsend, "Formation of planar waveguides in bismuth germanate by ^{4}He$^+$ ion implantation," J. Phys. D **22**, 1354–1357 (1989).

29. S. M. Mahdavi and P. D. Townsend, "Optical effects of defect diffusion in Bi$_4$Ge$_3$O$_{12}$ and Bi$_{12}$GeO$_{20}$ produced by ion implantation," J. Chem. Soc. Faraday Trans. **86**, 1287–1291 (1990).

30. J. Yang, C. Zhang, F. Chen, S. Akhmadaliev, and S. Q. Zhou, "Planar optical waveguides in Bi$_4$Ge$_3$O$_{12}$ crystal fabricated by swift heavy-ion irradiation," Appl. Opt. **50**, 6678–6681 (2011).

31. I. Bányász, S. Berneschi, N. Q. Khánh, T. Lohner, K. Lengyel, M. Fried, Á. Péter, P. Petrik, Z. Zolnai, A. Watterich, G. Nunzi-Conti, S. Pelli, and G. C. Righini, "Formation of slab waveguides in eulytine type BGO and CaF$_2$ crystals by implantation of MeV nitrogen ions," Nucl. Instrum. Methods Phys. Res., Sect. B **286**, 80–84 (2012).

32. B. Qian, Y. Liao, G. P. Dong, F. F. Luo, L. B. Su, S. Z. Sun, and J. R. Qiu, "Femtosecond laser-written waveguides in a bismuth germanate single crystal," Chin. Phys. Lett. **26**, 070601 (2009).

33. C. Zhang, N. N. Dong, J. Yang, F. Chen, J. R. Vázquez de Aldana, and Q. M. Lu, "Channel waveguide lasers in Nd:GGG crystals fabricated by femtosecond laser inscription," Opt. Express **19**, 12503–12508 (2011).

34. G. A. Torchia, P. F. Meilán, A. Rodenas, D. Jaque, C. Mendez, and L. Roso, "Femtosecond laser written surface waveguides fabricated in Nd:YAG ceramics," Opt. Express **15**, 13266–13271 (2007).

35. http://www.rsoftdesign.com.

36. D. Yevick and W. Bardyszewiski, "Correspondence of variational finite-difference (relaxation) and imaginary-distance propagation methods for modal analysis," Opt. Lett. **17**, 329–330 (1992).

37. Q. An, Y. Ren, Y. Jia, J. Rodríguez Vázquez de Aldana, and F. Chen, "Mid-infrared waveguides in zinc sulfide crystal," Opt. Mater. Express **3**, 466–471 (2013).

38. R. Osellame, G. Cerullo, and R. Ramponi, *Femtosecond Laser Micromachining* (Springer-Verlag, 2012).